

MASTER

CONF-8509196--2

ELECTRON-ION COLLISIONS IN THE AVERAGE-CONFIGURATION
DISTORTED-WAVE APPROXIMATION[†]

DE86 007568

Michael S. Pindzola,^{*} Donald C. Griffin,^{**} and
Christopher Bottcher

Physics Division, Oak Ridge National Laboratory,
Oak Ridge, TN 37831

ABSTRACT

Explicit expressions for the electron-impact excitation, ionization, and resonant-recombination cross sections are derived in the average-configuration distorted-wave approximation. Calculations using these expressions are applied to several types of phenomena in electron-ion scattering where comparison with other theoretical methods and experimental measurements can be made.

I. INTRODUCTION

The theoretical study of electron-ion scattering processes not only extends our understanding of atomic many-body structure and collision dynamics but also has important applications in laboratory and astrophysical plasma research. Even with the advent of high-speed computational machines a detailed knowledge of the time evolution of a many-particle fermion system remains elusive. In the spirit of a NATO Advanced Study a simple introductory approach to the electron-ion scattering problem is presented based on the single-configuration Hartree-Fock model of the atom. In the following sections explicit expressions are derived and numerical results are calculated in the average-configuration distorted-wave approximation for the electron-impact excitation, ionization and resonant-recombination cross sections.

The review is begun in Sect. II by deriving in the uncoupled representation the average-configuration, or array-averaged, radiative transition rate. The same methods are then applied in Sect. III to obtain expressions for the average-configuration autoionization transition

[†]Research supported by the Office of Fusion Energy, U.S. Department of Energy, under Contract No. DE-AC05-84OR21400 with Martin Marietta Energy Systems, Inc.

^{*}Department of Physics, Auburn University, Auburn, AL 36849.

^{**}Department of Physics, Rollins College, Winter Park, FL 32789.

rate. In Sect. IV the average-configuration resonant-recombination cross section is found by applying the principle of detailed balancing to the autoionization rates of Sect. III. Successive substitutions of continuum orbitals for bound orbitals in Sects. V and VI completes the derivation of both the average-configuration excitation and ionization cross sections. The results of calculations using the average-configuration electron-ion scattering cross sections are presented in Sect. VII, where comparisons with both more detailed theoretical methods and experimental measurements are made. Despite its simplicity the average-configuration distorted-wave approximation proves quite useful and sometimes surprisingly accurate in predicting various electron-ion scattering processes.

II. AVERAGE-CONFIGURATION RADIATIVE RATE

Besides forming a simple introduction to the averaging methods, the average-configuration radiative rate proves quite useful in calculating branching ratios for various electron-ion scattering processes. From time-dependent perturbation theory the radiative transition rate from a state i of the initial level to a state f of the final level is given by

$$A_r = \frac{4\omega^3}{3c^3} \left| \langle \gamma_f J_f M_f | \sum_{i=1}^N \vec{r}_i | \gamma_i J_i M_i \rangle \right|^2, \quad (1)$$

where ω is the transition frequency, c is the speed of light and atomic units are used (1 a.u. = 27.212 eV). The labels J and M are the total angular momentum quantum numbers for the N electron state, while γ represents all other quantum numbers needed to complete the specification. The wavefunction $\langle \vec{r} | \gamma J M \rangle$ is chosen to be a linear combination of antisymmetrized product states where the single-particle spin-orbitals are given by

$$\langle \vec{r} | n \ell m \ell m_s \rangle = \frac{P_{n\ell}(r)}{r} Y_{\ell m \ell}(\theta, \phi) \chi_{m_s}(\sigma). \quad (2)$$

When the many-particle states $|\gamma J M\rangle$ involved in a transition can be adequately represented by single configurations, it is useful to define an average-configuration radiative transition rate by¹

$$A_r = \frac{4\bar{\omega}^3}{3c^3} \frac{\sum_{\gamma_f J_f M_f} \sum_{\gamma_i J_i M_i} \left| \langle \gamma_f J_f M_f | \sum_{i=1}^N \vec{r}_i | \gamma_i J_i M_i \rangle \right|^2}{\sum_{\gamma_i J_i} (2J_i + 1)}, \quad (3)$$

where $\bar{\omega}$ is the average transition frequency. The average rate \bar{A}_r can be used, for instance, in analyzing optical spectra in those special cases where individual lines are not resolved.

For a given transition between configurations

$$(n_1 \ell_1)^{q_1-1} (n_2 \ell_2)^{q_2} \rightarrow (n_1 \ell_1)^{q_1} (n_2 \ell_2)^{q_2-1}, \quad (4)$$

where q is the subshell occupation number, \bar{A}_r may be evaluated using any convenient angular momentum coupling scheme. An example of Eq. (4) is the transition $2s2p^2 \rightarrow 2s^22p$, where $q_1 = q_2 = 2$. It is especially instructive and quite simple, however, to evaluate \bar{A}_r in the uncoupled

representation. For a radiative transition involving the active orbitals $n_2 l_2 \rightarrow n_1 l_1$, the average rate \bar{A}_T of Eq. (3) may also be written as

$$\bar{A}_T = \frac{4\bar{\omega}^3}{3c^3} \frac{N_t(I \rightarrow F)}{G_I} |\langle n_1 l_1 | \vec{r} | n_2 l_2 \rangle|^2_{\text{avg}} \quad , \quad (5)$$

where G_I is the total number of states in the initial configuration, $N_t(I \rightarrow F)$ is the total number of single-particle transitions between the initial and final configurations, and $|\langle n_1 l_1 | \vec{r} | n_2 l_2 \rangle|^2_{\text{avg}}$ is the average square of the single-particle dipole matrix element. The initial configuration statistical weight is given by

$$G_I = \binom{4l_1 + 2}{q_1 - 1} \binom{4l_2 + 2}{q_2} \quad , \quad (6)$$

where $\binom{n}{m} = n! / [n-m]! m!$ is the binomial coefficient. The total number of single-particle transitions is given by

$$N_t(I \rightarrow F) = q_1 \binom{4l_1 + 2}{q_1} q_2 \binom{4l_2 + 2}{q_2} \quad , \quad (7)$$

An easy way to verify Eq. (7) is to try an example, like $2s \ 2p^2 \rightarrow 2s^2 \ 2p$. The active orbitals are $2p \rightarrow 2s$. There are $\binom{6}{2} = 15$ possible uncoupled states

$$(2p m_l m_s, 2p m_l' m_s')$$

in the active subshell of the initial configuration which can make transitions to the $\binom{2}{2} = 1$ possible uncoupled state

$$(2s m_l m_s, 2s m_l' m_s')$$

in the active subshell of the final configuration. Since there are 2 single-particle states in each of the uncoupled states in the initial active subshell and 2 single-particle states in the uncoupled state in the final active subshell, the total number of single-particle transitions is $(2)(15)(2)(1) = 60$.

The average square of the single-particle dipole matrix element is defined by

$$|\langle n_1 l_1 | \vec{r} | n_2 l_2 \rangle|^2_{\text{avg}} = \frac{\sum_{m_l_1, m_l_2} \sum_{m_s_1, m_s_2} \delta_{m_s_1, m_s_2} |\langle n_1 l_1 m_l_1 | \vec{r} | n_2 l_2 m_l_2 \rangle|^2}{(4l_1 + 2)(4l_2 + 2)} \quad . \quad (8)$$

If we write \vec{r} in terms of the $\kappa = 1$ spherical harmonic tensor,

$$\vec{r} = r \sum_{\lambda=-1}^1 C_{\lambda}^{(1)} \quad , \quad (9)$$

then the dipole matrix element of Eq. (8) is given by

$$\begin{aligned}
& \langle n_1 \ell_1 m_{\ell_1} | \vec{r} | n_2 \ell_2 m_{\ell_2} \rangle \\
&= D(12) \sum_{\lambda} \langle n_1 \ell_1 m_{\ell_1} | C^{(1)} | n_2 \ell_2 m_{\ell_2} \rangle \\
&= D(12) \sum_{\lambda} (-1)^{m_{\ell_2}} \sqrt{(2\ell_1+1)(2\ell_2+1)} \begin{pmatrix} \ell_1 & 1 & \ell_2 \\ 0 & 0 & 0 \end{pmatrix} \begin{pmatrix} \ell_1 & 1 & \ell_2 \\ m_{\ell_1} & \lambda & -m_{\ell_2} \end{pmatrix}, \quad (10)
\end{aligned}$$

where the radial dipole matrix element is given by

$$D(12) = \int_0^{\infty} P_{n_1 \ell_1}(r) r P_{n_2 \ell_2}(r) dr \quad . \quad (11)$$

After squaring the dipole matrix element of Eq. (10), substituting into Eq. (8), and then making use of the properties of sums over 3-j symbols, one obtains

$$|\langle n_1 \ell_1 | \vec{r} | n_2 \ell_2 \rangle|^2_{\text{avg}} = \frac{2\lambda_{>} [D(12)]^2}{(4\ell_1+2)(4\ell_2+2)} \quad . \quad (12)$$

where $\lambda_{>} = \max \{ \ell_1, \ell_2 \}$.

Substituting G_I of Eq. (6), $N_{\tau}(I \rightarrow F)$ of Eq. (7), and $|\langle n_1 \ell_1 | \vec{r} | n_2 \ell_2 \rangle|^2_{\text{avg}}$ of Eq. (12) into Eq. (5) for \bar{A}_{τ} , we obtain

$$\bar{A}_{\tau} = \frac{8\bar{\omega}^3}{3c^3} \frac{q_1 q_2 \begin{pmatrix} 4\ell_1 + 2 \\ q_1 \end{pmatrix} \begin{pmatrix} 4\ell_2 + 2 \\ q_2 \end{pmatrix}}{\begin{pmatrix} 4\ell_1 + 2 \\ q_1 - 1 \end{pmatrix} \begin{pmatrix} 4\ell_2 + 2 \\ q_2 \end{pmatrix}} \frac{\lambda_{>} [D(12)]^2}{(4\ell_1 + 2)(4\ell_2 + 2)} \quad , \quad (13)$$

or more simply

$$\bar{A}_{\tau} = \frac{8\bar{\omega}^3}{3c^3} q_2 \frac{(4\ell_2 + 3 - q_1)}{(4\ell_1 + 2)(4\ell_2 + 2)} \lambda_{>} [D(12)]^2 \quad . \quad (14)$$

The configuration energies and bound radial orbitals needed to complete the evaluation of \bar{A}_{τ} for any atomic system may be obtained from the atomic structure code of one's choice, such as Cowan's RCN program¹ or Fischer's MCHF program.²

III. AVERAGE-CONFIGURATION AUTOIONIZATION RATE

The autoionization transition rate from a state i of an initial level of an $N+1$ electron ion to a state f of the final level of an N electron ion is given by

$$A_a = \frac{4}{k_f} |\langle \gamma_f J_f M_f | \sum_{i < j = 1}^{N+1} v_{ij} | \gamma_i J_i M_i \rangle|^2 \quad , \quad (15)$$

where $v_{ij} = 1/|\vec{r}_i - \vec{r}_j|$ and k_f is the wavenumber of the continuum final state $|\gamma_f J_f M_f\rangle$, whose asymptotic form is one times a sine function. In the single configuration approximation, an average-configuration autoionization rate is defined by¹

$$\bar{A}_a = \frac{4}{\bar{k}_f} \frac{\sum_{\gamma_f J_f M_f} \sum_{\gamma_1 J_1 M_1} |\langle \gamma_f J_f M_f | \sum_{1 \leq j=1}^{N+1} v_{1j} | \gamma_1 J_1 M_1 \rangle|^2}{\sum_{\gamma_1 J_f} (2J_1 + 1)}, \quad (16)$$

where \bar{k}_f is the average wavenumber. As previously noted,³ for the first of two types of transitions between configurations given by

$$(n_1 l_1)^{q_1} (n_2 l_2)^{q_2} (n_3 l_3)^{q_3} \rightarrow (n_1 l_1)^{q_1+1} (n_2 l_2)^{q_2-1} (n_3 l_3)^{q_3-1} k_4 l_4, \quad (17)$$

\bar{A}_a may be evaluated using any convenient angular momentum coupling scheme. An example of Eq. (17) is the transition $2p^5 3s^2 3p \rightarrow 2p^6 3s k l$, where $q_1 = 5$, $q_2 = 2$ and $q_3 = 1$. For an autoionization transition involving the active orbitals $(n_2 l_2, n_3 l_3) \rightarrow (n_1 l_1, k_4 l_4)$, the average rate \bar{A}_a in the uncoupled representation may also be written as

$$\bar{A}_a = \frac{4}{k_4} \frac{N_T(I \rightarrow F)}{G_I} |\langle n_1 l_1 \tilde{k}_4 l_4 | v | n_2 l_2 n_3 l_3 \rangle|^2_{\text{avg}}, \quad (18)$$

where G_I is again the total number of states in the initial configuration, $N_T(I \rightarrow F)$ is the total number of transitions between the initial and final configurations, and $|\langle n_1 l_1 \tilde{k}_4 l_4 | v | n_2 l_2 n_3 l_3 \rangle|^2_{\text{avg}}$ is the average square of the two-body Coulomb matrix element. The initial configuration statistical weight is given by

$$G_I = \binom{4l_1 + 2}{q_1} \binom{4l_2 + 2}{q_2} \binom{4l_3 + 2}{q_3}, \quad (19)$$

while the total number of transitions is given by

$$N_T(I \rightarrow F) = (q_1 + 1) \binom{4l_1 + 2}{q_1 + 1} q_2 \binom{4l_2 + 2}{q_2} q_3 \binom{4l_3 + 2}{q_3} \binom{4l_4 + 2}{1}, \quad (20)$$

in analogy with Eqs. (6) and (7) of Sect. I.

The average square of the Coulomb matrix element may be separated into direct, exchange and cross terms,

$$\begin{aligned} & |\langle n_1 l_1 \tilde{k}_4 l_4 | v | n_2 l_2 n_3 l_3 \rangle|^2_{\text{avg}} \\ &= |\langle n_1 l_1 k_4 l_4 | v | n_2 l_2 n_3 l_3 \rangle|^2_{\text{avg}} + |\langle k_4 l_4 n_1 l_1 | v | n_2 l_2 n_3 l_3 \rangle|^2_{\text{avg}} \\ &\quad - 2 |\langle n_1 l_1 k_4 l_4 | v | n_2 l_2 n_3 l_3 \rangle \langle k_4 l_4 n_1 l_1 | v | n_2 l_2 n_3 l_3 \rangle|_{\text{avg}}. \end{aligned} \quad (21)$$

The average direct term is defined by

$$\begin{aligned} & |\langle n_1 l_1 k_4 l_4 | v | n_2 l_2 n_3 l_3 \rangle|^2_{\text{avg}} \\ &= \sum_{\substack{m_{l_1}, m_{l_2} \\ m_{l_3}, m_{l_4}}} \sum_{\substack{m_{s_1}, m_{s_2} \\ m_{s_3}, m_{s_4}}} \frac{\delta_{m_{s_1}, m_{s_2}} \delta_{m_{s_3}, m_{s_4}} |\langle n_1 l_1 m_{l_1} k_4 l_4 m_{l_4} | v | n_2 l_2 m_{l_2} n_3 l_3 m_{l_3} \rangle|^2}{(4l_1 + 2) (4l_2 + 2) (4l_3 + 2) (4l_4 + 2)}. \end{aligned} \quad (22)$$

If we write v in terms of a product of spherical harmonic tensors,

$$v = \sum_{\kappa} \frac{r_{<}^{\kappa}}{r_{>}^{\kappa+1}} \sum_{\lambda=-\kappa}^{\kappa} (-1)^{\lambda} C_{-\lambda}^{(\kappa)} C_{\lambda}^{(\kappa)}, \quad (23)$$

then the direct matrix element of Eq. (22) is given by

$$\begin{aligned} & \langle n_1 l_1 m_{l_1} k_4 l_4 m_{l_4} | v | n_2 l_2 m_{l_2} n_3 l_3 m_{l_3} \rangle \\ &= \sum_{\kappa} R^{\kappa}(14;23) \sum_{\lambda} (-1)^{\lambda} \langle n_1 l_1 m_{l_1} k_4 l_4 m_{l_4} | C_{-\lambda}^{(\kappa)} C_{\lambda}^{(\kappa)} | n_2 l_2 m_{l_2} n_3 l_3 m_{l_3} \rangle \\ &= \sum_{\kappa} R^{\kappa}(14;23) \sum_{\lambda} (-1)^{\lambda} (-1)^{m_{l_2}+m_{l_3}} \sqrt{(2l_1+1)(2l_2+1)(2l_3+1)(2l_4+1)} \\ & \quad \begin{pmatrix} l_1 & \kappa & l_2 \\ 0 & 0 & 0 \end{pmatrix} \begin{pmatrix} l_3 & \kappa & l_4 \\ 0 & 0 & 0 \end{pmatrix} \begin{pmatrix} l_1 & \kappa & l_2 \\ -m_{l_1} & -\lambda & m_{l_2} \end{pmatrix} \begin{pmatrix} l_3 & \kappa & l_4 \\ -m_{l_3} & \lambda & m_{l_4} \end{pmatrix}, \quad (24) \end{aligned}$$

where the radial Slater integral is given by

$$R^{\kappa}(14;23) = \int_0^{\infty} \int_0^{\infty} P_{n_1 l_1}(r) P_{k_4 l_4}(r') \frac{r_{<}^{\kappa}}{r_{>}^{\kappa+1}} P_{n_2 l_2}(r) P_{n_3 l_3}(r') dr dr'. \quad (25)$$

After squaring the direct matrix element of Eq. (24), substituting into Eq. (22), and then making use of the properties of sums over 3-j symbols, one obtains

$$\begin{aligned} & |\langle n_1 l_1 k_4 l_4 | v | n_2 l_2 n_3 l_3 \rangle|_{\text{avg}}^2 \\ &= \frac{1}{4} \sum_{\kappa} \begin{pmatrix} l_1 & \kappa & l_2 \\ 0 & 0 & 0 \end{pmatrix}^2 \begin{pmatrix} l_3 & \kappa & l_4 \\ 0 & 0 & 0 \end{pmatrix}^2 \frac{[R^{\kappa}(14;23)]^2}{(2\kappa+1)}. \quad (26) \end{aligned}$$

The derivation of the average square of the exchange and cross terms of Eq. (21) proceeds in a similar manner to that of the direct term.

Substituting G_I of Eq. (19), $N_{\ell}(I \rightarrow F)$ of Eq. (20), and the complete expression for $|\langle n_1 l_1 k_4 l_4 | v | n_2 l_2 n_3 l_3 \rangle|_{\text{avg}}^2$ into Eq. (18) for \bar{A}_a , we obtain

$$\bar{A}_a = \frac{(q_1+1) q_2 q_3 \begin{pmatrix} 4l_1+2 \\ q_1+1 \end{pmatrix} \begin{pmatrix} 4l_2+2 \\ q_2 \end{pmatrix} \begin{pmatrix} 4l_3+2 \\ q_3 \end{pmatrix} \begin{pmatrix} 4l_4+2 \\ 1 \end{pmatrix} M(14;23)}{\bar{k}_4 \begin{pmatrix} 4l_1+2 \\ q_1 \end{pmatrix} \begin{pmatrix} 4l_2+2 \\ q_2 \end{pmatrix} \begin{pmatrix} 4l_3+2 \\ q_3 \end{pmatrix}}, \quad (27)$$

where

$$\begin{aligned}
 M(14;23) = & \sum_{\kappa} \begin{pmatrix} \ell_1 & \kappa & \ell_2 \\ 0 & 0 & 0 \end{pmatrix}^2 \begin{pmatrix} \ell_3 & \kappa & \ell_4 \\ 0 & 0 & 0 \end{pmatrix}^2 \frac{[R^{\kappa}(14;23)]^2}{(2\kappa+1)} \\
 & + \sum_{\kappa'} \begin{pmatrix} \ell_1 & \kappa' & \ell_3 \\ 0 & 0 & 0 \end{pmatrix}^2 \begin{pmatrix} \ell_2 & \kappa' & \ell_4 \\ 0 & 0 & 0 \end{pmatrix}^2 \frac{[R^{\kappa'}(41;23)]^2}{(2\kappa'+1)} \quad (28) \\
 & - \sum_{\kappa} \sum_{\kappa'} (-1)^{\kappa+\kappa'} \begin{Bmatrix} \ell_1 & \ell_2 & \kappa \\ \ell_4 & \ell_3 & \kappa' \end{Bmatrix} \begin{pmatrix} \ell_1 & \kappa & \ell_2 \\ 0 & 0 & 0 \end{pmatrix} \begin{pmatrix} \ell_3 & \kappa & \ell_4 \\ 0 & 0 & 0 \end{pmatrix} \begin{pmatrix} \ell_1 & \kappa' & \ell_3 \\ 0 & 0 & 0 \end{pmatrix} \begin{pmatrix} \ell_2 & \kappa' & \ell_4 \\ 0 & 0 & 0 \end{pmatrix} \\
 & R^{\kappa}(14;23) R^{\kappa'}(41;23) ,
 \end{aligned}$$

or more simply

$$\bar{A}_a = q_2 q_3 \frac{(4\ell_1 + 2 - q_1) (4\ell_4 + 2) M(14;23)}{\bar{k}_4} . \quad (29)$$

The second of the two types of transitions between configurations is given by

$$(n_1 \ell_1)^{q_1} (n_2 \ell_2)^{q_2} \rightarrow (n_1 \ell_1)^{q_1+1} (n_2 \ell_2)^{q_2-2} k_3 \ell_3 . \quad (30)$$

An example of Eq. (30) is the transition $2p^5 3s^2 \rightarrow 2p^6 k\ell$; where $q_1 = 5$ and $q_2 = 2$. Following the same steps as outlined above the autoionization rate is given by

$$\bar{A}_a = q_2 (q_2 - 1) \frac{(4\ell_1 + 2 - q_1) (4\ell_2 + 2) (4\ell_3 + 2) M'(13;22)}{\bar{k}_3 (4\ell_2 + 1)} , \quad (31)$$

where

$$\begin{aligned}
 M'(13;22) = & \sum_{\kappa} \begin{pmatrix} \ell_1 & \kappa & \ell_2 \\ 0 & 0 & 0 \end{pmatrix}^2 \begin{pmatrix} \ell_2 & \kappa & \ell_3 \\ 0 & 0 & 0 \end{pmatrix}^2 \frac{[R^{\kappa}(13;22)]^2}{(2\kappa+1)} \quad (32) \\
 & - \frac{1}{2} \sum_{\kappa} \sum_{\kappa'} (-1)^{\kappa+\kappa'} \begin{Bmatrix} \ell_1 & \ell_2 & \kappa \\ \ell_3 & \ell_2 & \kappa' \end{Bmatrix} \begin{pmatrix} \ell_1 & \kappa & \ell_2 \\ 0 & 0 & 0 \end{pmatrix} \begin{pmatrix} \ell_2 & \kappa & \ell_3 \\ 0 & 0 & 0 \end{pmatrix} \begin{pmatrix} \ell_1 & \kappa' & \ell_2 \\ 0 & 0 & 0 \end{pmatrix} \begin{pmatrix} \ell_2 & \kappa' & \ell_3 \\ 0 & 0 & 0 \end{pmatrix} \\
 & R^{\kappa}(13;22) R^{\kappa'}(13;22) .
 \end{aligned}$$

The configuration energies and bound radial orbitals needed to evaluate the two types of \bar{A}_a for any atomic system may be obtained from any convenient atomic structure code. Computer subroutines can provide rapid evaluation of the 3-j and 6-j symbols and numerical evaluation of the radial Slater integrals is straightforward. The continuum radial orbitals needed to complete the evaluation of \bar{A}_a may be obtained by solving the radial Schrodinger equation in the distorted-wave approximation. For rapid evaluation of many continuum orbitals a local distorting potential constructed in a semiclassical exchange approximation⁴ has proved quite useful. This exchange term simplifies the solution of the differential equation and generally gives results in close agreement with results obtained from a full non-local Hartree-Fock continuum

calculation. As will be seen in the next three sections, the expressions for M and M' are the main working equations for the average-configuration method applied to electron scattering processes.

IV. AVERAGE-CONFIGURATION RECOMBINATION CROSS SECTION

The inverse of the autoionizing transition between configurations of Eq. (17) is the recombination process of the type

$$(n_1 l_1)^{q_1+1} (n_2 l_2)^{q_2-1} (n_3 l_3)^{q_3-1} k_1 l_1 \rightarrow (n_1 l_1)^{q_1} (n_2 l_2)^{q_2} (n_3 l_3)^{q_3}, \quad (33)$$

where we identify the incident electron by replacing $k_4 l_4 \rightarrow k_1 l_1$. The recombination process involves the active orbitals $(n_1 l_1, k_1 l_1) \rightarrow (n_2 l_2, n_3 l_3)$. From the principle of detailed balancing the average-configuration recombination cross section is given by¹

$$\bar{\sigma}_{\text{recomb}} = \frac{2\pi^2}{k_1^2 \Delta\epsilon} \sum_{l_1} \frac{G_I}{2G_F} \bar{A}_a, \quad (34)$$

where G_I is given by Eq. (19), \bar{A}_a is given by Eq. (29),

$$G_F = \begin{pmatrix} 4l_1 + 2 \\ q_1 + 1 \end{pmatrix} \begin{pmatrix} 4l_2 + 2 \\ q_2 - 1 \end{pmatrix} \begin{pmatrix} 4l_3 + 2 \\ q_3 - 1 \end{pmatrix}, \quad (35)$$

and $\Delta\epsilon$ is an energy width larger than the largest resonance width. Substituting the expressions for G_I , G_F , and \bar{A}_a into Eq. (34) gives

$$\bar{\sigma}_{\text{recomb}} = \frac{2\pi^2}{k_1^3 \Delta\epsilon} (q_1 + 1) (4l_3 + 3 - q_3) (4l_2 + 3 - q_2) \sum_{l_1} (2l_1 + 1) M(23; 11). \quad (36)$$

The inverse of Eq. (30) is the recombination process of the type

$$(n_1 l_1)^{q_1+1} (n_2 l_2)^{q_2-2} k_1 l_1 \rightarrow (n_1 l_1)^{q_1} (n_2 l_2)^{q_2}. \quad (37)$$

The recombination process involves the active orbitals $(n_1 l_1, k_1 l_1) \rightarrow (n_2 l_2)^2$. The average-configuration recombination cross section is given by

$$\bar{\sigma}_{\text{recomb}} = \frac{2\pi^2}{k_1^3 \Delta\epsilon} \frac{(q_1 + 1) (4l_2 + 4 - q_2) (4l_2 + 3 - q_2) (4l_2 + 2)}{(4l_2 + 1)} \sum_{l_1} (2l_1 + 1) M'(22; 11). \quad (38)$$

V. AVERAGE-CONFIGURATION EXCITATION CROSS SECTION

A slight modification of the recombination process of Eq. (33) yields the electron excitation scattering process

$$(n_1 l_1)^{q_1+1} (n_2 l_2)^{q_2-1} k_1 l_1 \rightarrow (n_1 l_1)^{q_1} (n_2 l_2)^{q_2} k_f l_f, \quad (39)$$

where we identify the scattered electron by replacing $n_3 l_3 \rightarrow k_f l_f$ and substituting $q_3 = 1$. The excitation process involves the active electrons $(n_1 l_1, k_1 l_1) \rightarrow (n_2 l_2, k_f l_f)$. The average-configuration excitation cross section is given by

$$\bar{\sigma}_{\text{exc}} = \rho_f \Delta \varepsilon \sum_{\lambda_f} \bar{\sigma}_{\text{recomb}} , \quad (40)$$

where the density of states ρ_f equals $2/\pi k_f$ for our choice of continuum normalization. Substituting for $\bar{\sigma}_{\text{recomb}}$ from Eq. (36) one finds that

$$\bar{\sigma}_{\text{exc}} = \frac{8\pi}{k_i^3 k_f} (q_1+1) (4\lambda_2+3-q_2) \sum_{\lambda_1, \lambda_f} (2\lambda_1+1) (2\lambda_f+1) M(2f; l_1) . \quad (41)$$

VI. AVERAGE-CONFIGURATION IONIZATION CROSS SECTION

A slight modification of the excitation process of Eq. (39) yields the electron ionization scattering process

$$(n_1 \lambda_1)^{q_1+1} k_i \lambda_i \rightarrow (n_1 \lambda_1)^{q_1} k_e \lambda_e k_f \lambda_f , \quad (42)$$

where we identify the ejected electron by replacing $n_2 \lambda_2 \rightarrow k_e \lambda_e$ and substituting $q_2 = 1$. The ionization process involves the active electrons $(n_1 \lambda_1, k_i \lambda_i) \rightarrow (k_e \lambda_e, k_f \lambda_f)$. The average-configuration differential ionization cross section is given by

$$\frac{d\bar{\sigma}_{\text{ion}}}{d\varepsilon} = \rho_e \sum_{\lambda_e} \bar{\sigma}_{\text{exc}} , \quad (43)$$

where $\varepsilon = \bar{k}_e^2/2$ is the ejected electron energy. Substituting for $\bar{\sigma}_{\text{exc}}$ from Eq. (41) one finds that

$$\frac{d\bar{\sigma}_{\text{ion}}}{d\varepsilon} = \frac{32}{k_i^3 k_e k_f} (q_1+1) \sum_{\lambda_1, \lambda_f, \lambda_e} (2\lambda_1+1) (2\lambda_e+1) (2\lambda_f+1) M(ef; l_1) . \quad (44)$$

The total average-configuration ionization cross section is given by

$$\bar{\sigma}_{\text{ion}} = \int_0^{E_{\text{max}}/2} \frac{d\bar{\sigma}_{\text{ion}}}{d\varepsilon} d\varepsilon , \quad (45)$$

where $E_{\text{max}} = (k_e^2 + k_f^2)/2$. Due to the presence of two outgoing continuum orbitals the phase of the interference term in Eq. (28) is arbitrary. The maximum interference approximation of Peterkop⁵ takes the negative of the absolute value of the third term on the right hand side of Eq. (28).

VII. CALCULATIONS USING AVERAGE-CONFIGURATION SCATTERING CROSS SECTIONS

The average-configuration scattering cross sections find great utility in the study of electron-impact ionization of atomic ions. Consider the following processes for ionization of an atomic ion labeled A:



are compared with the 3-parameter semi-empirical Lotz formula⁷ and the experimental crossed-beams measurements of Mueller et al.⁸ The break in the theoretical curve at 80 eV is the onset of the 2s ionization. Although the remarkable agreement between theory and experiment in F^{2+} is not typical of other atomic ions, the direct ionization process seems to be described to fairly good accuracy by the average-configuration distorted-wave approximation of Eq. (45).

For electron-impact ionization of S^{4+} both the direct process and the excitation-autoionization process contribute to the total cross section. In Fig. 2 average-configuration excitation and ionization cross section calculations⁹ for the transitions

$$2p^6 3s 3p k_1 \lambda_1 \begin{cases} \rightarrow 2p^5 3s 3p^2 k_f \lambda_f , \\ \rightarrow 2p^5 3s 3p 3d k_f \lambda_f , \\ \rightarrow 2p^5 3s 3p 4p k_f \lambda_f , \\ \rightarrow 2p^5 3s 3p 4d k_f \lambda_f \end{cases} \quad (50)$$

and

$$2p^6 3s 3p k_1 \lambda_1 \begin{cases} \rightarrow 2p^6 3s k_e \lambda_e k_f \lambda_f , \\ \rightarrow 2p^6 3p k_e \lambda_e k_f \lambda_f , \\ \rightarrow 2p^5 3s 3p k_e \lambda_e k_f \lambda_f , \end{cases} \quad (51)$$

are compared with the experimental crossed-beams measurements of Howald et al.¹⁰ The break in the theoretical curve at 170 eV is the onset of the excitation-autoionization processes. Besides the remarkable agreement between theory and experiment, one of the interesting features of the S^{4+} study is confirmation that the metastable $2p^6 3s 3p$ configuration dominates the composition of the ion beam, since the agreement between theory and experiment for ionization from the $2p^6 3s^2$ configuration is not as good. Note also that 2p direct ionization would contribute to the formation of S^{6+} except for the fact that a majority of the states of the $2p^5 3s 3p$ configuration live long enough to be detected as S^{5+} .

For electron-impact ionization of Ti^{3+} the excitation-autoionization process dominates the cross section. In Fig. 3 average-configuration excitation and ionization cross section calculations¹¹ for the transitions

$$3p^6 3d k_1 \lambda_1 \rightarrow 3p^5 3d^2 k_f \lambda_f , \quad (52)$$

and

$$3p^6 3d k_1 \lambda_1 \rightarrow 3p^6 k_e \lambda_e k_f \lambda_f , \quad (53)$$

are compared with an intermediate-coupled level to level distorted-wave calculation¹² and the experimental crossed-beams measurements of Falk et al.¹³ The $3p \rightarrow 3d$ average-configuration excitation cross section for Ti^{3+} has a total threshold value of $179 \times 10^{-18} \text{ cm}^2$ distributed over 45 different levels. Atomic structure calculations¹ show that only 6 of the 45 levels are autoionizing. The average-configuration curve in Fig. 3 is a statistical distribution of the collision strength to those 6 levels. The more detailed level to level calculation¹² finds instead that the 6 autoionizing levels carry much more collision strength than a

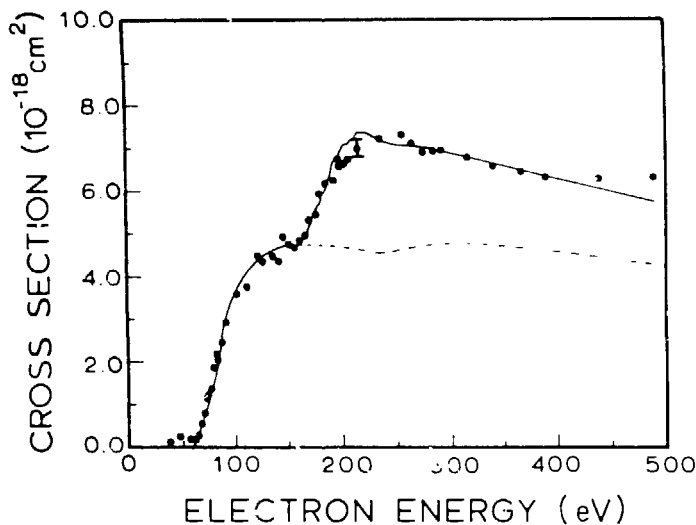


Fig. 2. Electron-impact ionization of S⁴⁺. Solid curve: average-configuration distorted-wave calculation for the total ionization including excitation-autoionization of the 2p⁶3s3p configuration (Ref. 9); dashed curve: direct ionization only; experimental data are from Howard et al. (Ref. 10).

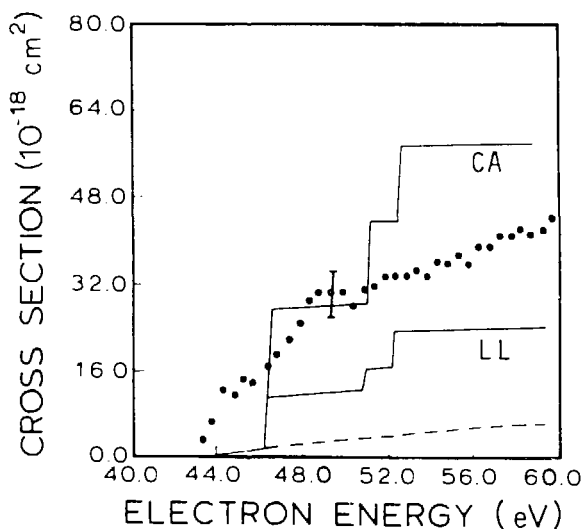


Fig. 3. Near threshold electron-impact ionization of Ti³⁺. Solid curve marked CA: average-configuration distorted-wave calculation for the total ionization including excitation-autoionization of the 3p⁶3d configuration (Ref. 11); solid curve marked LL: level to level distorted-wave calculation for the total ionization (Ref. 12); dashed curve: direct ionization only; experimental data are from Falk et al. (Ref. 13).

statistical distribution would indicate, although the total value of $179 \times 10^{-18} \text{ cm}^2$ is about the same. The average-configuration distorted-wave method may be in substantial error for those atomic systems in which the levels of the dominant excitation-autoionization configuration straddle the ionization threshold. Note that at higher energies the excitation transitions

$$3p^6 3d \ k_1 \ell_1 \rightarrow 3p^5 3d 4 \ell \ k_f \ell_f \quad (54)$$

will certainly contribute to the total cross section, while on the other hand the 3p direct ionization contributes only to the formation of Ti^{5+} . Recent configuration-interaction level to level distorted-wave calculations¹⁴ and configuration-interaction close-coupling calculations^{15,16} have found that theory and experiment are in substantial agreement for Ti^{3+} .

For electron-impact ionization of Sb^{3+} the resonant-recombination double autoionization process contributes to the total ionization cross section. Associated with the dominant excitation-autoionization transition¹⁷

$$4d^1 0 5s^2 \ k_1 \ell_1 \rightarrow 4d^9 5s^2 4f \ k_f \ell_f , \quad (55)$$

are the resonant-recombination transitions

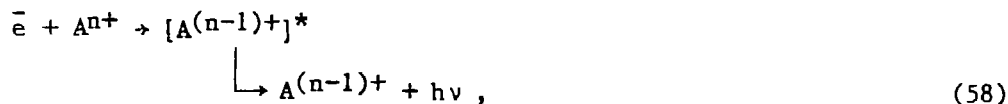
$$4d^1 0 5s^2 \ k_1 \ell_1 \rightarrow 4d^9 5s^2 4f n \ell . \quad (56)$$

The enhancement of the total ionization cross section below the energy threshold of the 4d \rightarrow 4f excitation is given by

$$\bar{\sigma}_{\text{rrda}} = \sum_{n\ell} \bar{\sigma}_{\text{recomb}}(n\ell) \bar{B}_{\text{da}}(n\ell) , \quad (57)$$

where $\bar{B}_{\text{da}}(n\ell)$ is the branching ratio for double autoionization. An average-configuration resonant-recombination cross section calculation for the 10d, with an energy bin width of 1 eV, yields $0.13 \times 10^{-18} \text{ cm}^2$.¹⁸ Combined with the many other n ℓ configurations the effect of the resonant-recombination process is to substantially enhance the total cross section below the 4d \rightarrow 4f threshold. Care must be taken, however, in computing the double autoionization branching ratio. For 4d⁹5s² 4f 10d the dominant decay mode is autoionization to the 4d⁹5s² 5d configuration, which is itself an autoionizing configuration. For many atomic systems the first step decay of the doubly-excited resonant configuration is to a bound configuration, thus \bar{B}_{da} is close to zero and no resonant-recombination enhancement occurs.

The process of the dielectronic recombination of an atomic ion labeled A:



can be described using the average-configuration transition rates and scattering cross sections of the previous sections. For dielectronic recombination of Mg^+ the resonant-recombination transitions are

$$2p^6 3s \ k_1 \ell_1 \rightarrow 2p^6 3p n \ell . \quad (59)$$

The average-configuration dielectronic recombination cross section is given by

$$\bar{\sigma}_{dr} = \sum_{n\ell} \bar{\sigma}_{\text{recomb}}(n\ell) \bar{B}_{rs}(n\ell), \quad (60)$$

where $\bar{B}_{rs}(n\ell)$ is the branching ratio for radiative stabilization. For Mg^+ $\bar{B}_{rs}(n\ell) \rightarrow 1$ as $n \rightarrow \infty$, thus the total dielectronic recombination cross section peaks at relatively high n values. In Fig. 4 an average-configuration dielectronic recombination cross section calculation¹⁹ is compared to an intermediate-coupled distorted-wave calculation²⁰ and the experimental crossed-beams measurements of Belic et al.²¹ Due to field ionization effects in the experiment only resonances with $n < 63$ are included in the calculations. The natural Rydberg spectrum of narrow peaks converging to the 3p ionization limit at 4.5 eV has been convoluted with a 0.3 eV Gaussian to simulate the experimental resolution. Although beyond the scope of this review, field mixing effects in the experiment can be incorporated¹⁹ in the average-configuration approximation by changing from a spherical to parabolic coordinate system for the Rydberg electron. The average-configuration results are about 25% high when compared to a more detailed intermediate-coupled matrix-diagonalized distorted-wave calculation.²⁰

Although of rather limited utility, the average-configuration scattering cross sections can be used in the study of electron-impact excitation of atomic ions. Consider the following processes for excitation of an atomic ion labeled A:

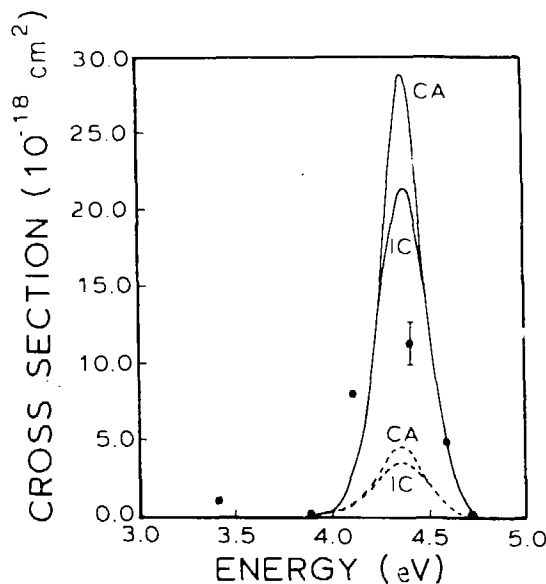


Fig. 4. Dielectronic recombination cross section for Mg^+ including all resonances with $n < 63$ convoluted with a 0.3 eV Gaussian. Solid curve marked CA: average-configuration distorted-wave calculation including complete field mixing (Ref. 19); solid curve marked IC: intermediate-coupled distorted-wave calculation at a field strength of 24 V/cm (Ref. 20); dashed curve marked CA: average-configuration distorted-wave calculation with no field mixing (Ref. 19); dashed curve marked IC: intermediate-coupled distorted-wave calculation at zero field strength (Ref. 20); experimental data are from Belic' et al. (Ref. 21).

$$e^- + A_i^{n+} \rightarrow A_f^{n+} + e^- , \quad (61)$$

and

$$e^- + A_i^{n+} \rightarrow [A^{(n-1)+}]^* \begin{array}{l} \downarrow \\ \rightarrow A_f^{n+} + e^- . \end{array} \quad (62)$$

The first process is direct $i \rightarrow f$ excitation and the second is resonant-recombination autoionization. These processes can sometimes be treated as independent.

For most applications excitation cross sections are needed for level to level or multiplet to multiplet transitions. The average-configuration method, however, can prove quite useful for survey work, analyzing complicated transition arrays in high Z atomic systems, and treating simple alkali-like atomic ions. For the electron-impact $2s \rightarrow 3s$ excitation of O^{5+} the direct excitation process is substantially enhanced by the resonant-recombination autoionization process. Associated with the excitation transition

$$1s^2 2s k_1 l_1 \rightarrow 1s^2 3s k_f l_f , \quad (63)$$

are the resonant-recombination transitions

$$1s^2 2s k_1 l_1 \begin{array}{l} \rightarrow 1s^2 3p n l \\ \rightarrow 1s^2 3d n l \\ \rightarrow 1s^2 4 l' n l . \end{array} \quad (64)$$

The enhancement of the excitation cross section for a single Rydberg series of doubly-excited configurations is given by

$$\bar{\sigma}_{rra} = \sum_{n\lambda} \sigma_{recomb}(n\lambda) \bar{B}_{a,f}(n\lambda) , \quad (65)$$

where $\bar{B}_{a,f}(n\lambda)$ is the branching ratio for single autoionization leaving the ion in the final configuration, in this case $1s^2 3s$. In Fig. 5 an average-configuration excitation cross section calculation for O^{5+} is presented.²² The natural spectrum of narrow peaks on top of the smooth background cross section has been convoluted with a 0.3 eV Gaussian to simulate a typical experimental resolution. Care must be taken again in computing the single autoionization branching ratio. Above the $1s^2 3p$ energy threshold at 83 eV, members of $1s^2 3d n l$ and $1s^2 4 l' n l$ sequences preferentially decay to the $1s^2 3p$ continuum. Thus large resonance enhancements of the excitation cross sections are confined primarily to the near-threshold energy region. Although not shown, comparison of $2s \rightarrow 3s$ average-configuration distorted-wave results with other more detailed close-coupling^{23,24} calculations is quite good.

VIII. CONCLUSIONS

The average-configuration scattering cross section equations derived in the preceding sections can quite easily be converted to machine code and implemented on any fairly large memory computer. They provide a useful theoretical tool for prediction of electron-impact excitation,

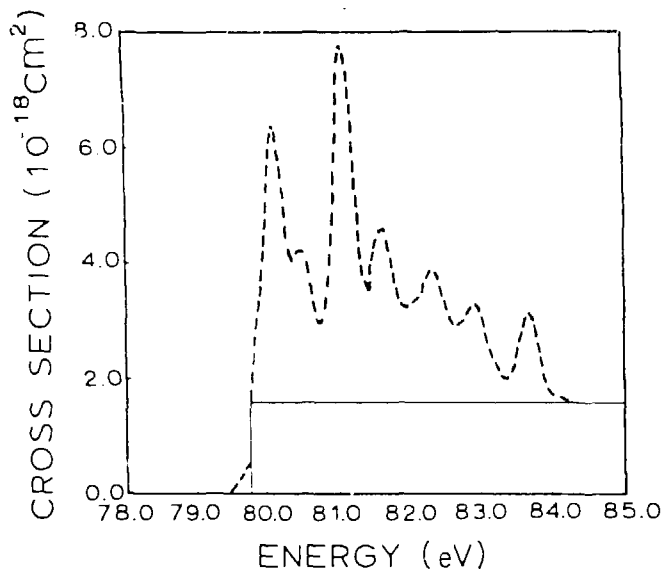


Fig. 5. Electron-impact $2s \rightarrow 3s$ excitation of O^{5+} . Dashed curve: average-configuration distorted-wave calculation for the total excitation including all resonances convoluted with a 0.3 eV Gaussian (Ref. 22); solid curve: direct excitation only.

ionization, and resonant-recombination processes. If used in conjunction with more detailed theoretical methods and new experimental techniques, they can greatly increase our understanding of the nature of electron-ion collisions.

ACKNOWLEDGMENTS

We wish to thank members of the ORNL-JILA experimental group, A. M. Howald et al. (Ref. 10), for providing us with their experimental data on S^{4+} before publication and for many valuable discussions. We also would like to acknowledge R. D. Cowan for providing us with a copy of his atomic-structure programs and a number of helpful conversations. Finally special thanks goes to D. H. Crandall for his interest and support of our theoretical efforts in electron-ion collision physics.

REFERENCES

1. R. D. Cowan, "The Theory of Atomic Structure and Spectra" (University of California, Berkeley, 1981).
2. C. F. Fischer, "The Hartree-Fock Method for Atoms" (Wiley, New York, 1977).
3. J. N. Gau and Y. Hahn, *J. Quant. Spectrosc. Radiat. Transfer* **23**, 121 (1980).
4. M. E. Riley and D. G. Truhlar, *J. Chem. Phys.* **63**, 2182 (1975).
5. R. K. Peterkop, *Zh. Eksp. Teor. Fiz.* **41**, 1938 (1961) [*Sov. Phys. JETP* **14**, 1377 (1962)].
6. S. M. Younger (private communication); see S. M. Younger, *Phys. Rev. A* **22**, 111 (1980), for a discussion of the numerical method.
7. W. Lotz, *Z. Phys.* **220**, 466 (1969).

8. D. W. Mueller, T. J. Morgan, G. H. Dunn, D. C. Gregory, and D. H. Crandall, *Phys. Rev. A* 31, 2905 (1985).
9. M. S. Pindzola, D. C. Griffin, and C. Bottcher (to be published).
10. A. M. Howald, D. C. Gregory, F. W. Meyer, R. A. Phaneuf, A. Müller, N. Djuric, and G. H. Dunn (to be published).
11. M. S. Pindzola, D. C. Griffin, C. Bottcher, D. C. Gregory, A. M. Howald, R. A. Phaneuf, D. H. Crandall, G. H. Dunn, D. W. Mueller, and T. J. Morgan, ORNL/TM-9436 (1985).
12. C. Bottcher, D. C. Griffin, and M. S. Pindzola, *J. Phys. B* 16, L65 (1983).
13. R. A. Falk, G. H. Dunn, D. C. Griffin, C. Bottcher, D. C. Gregory, D. H. Crandall, and M. S. Pindzola, *Phys. Rev. Lett.* 47, 494 (1981).
14. C. Bottcher, D. C. Griffin, and M. S. Pindzola (to be published).
15. P. G. Burke, W. C. Fon, and A. E. Kingston, *J. Phys. B* 17, L733 (1984).
16. R.J.W. Henry (private communication).
17. M. S. Pindzola, D. C. Griffin, and C. Bottcher, *Phys. Rev. A* 27, 2331 (1983).
18. D. C. Griffin, C. Bottcher, M. S. Pindzola, S. M. Younger, D. C. Gregory, and D. H. Crandall, *Phys. Rev. A* 29, 1729 (1984).
19. D. C. Griffin, M. S. Pindzola, and C. Bottcher, ORNL/TM-9478 (1985).
20. C. Bottcher, D. C. Griffin, and M. S. Pindzola (to be published).
21. D. C. Belic, G. H. Dunn, T. J. Morgan, D. W. Mueller, and C. Timmer, *Phys. Rev. Lett.* 50, 339 (1983).
22. M. S. Pindzola, D. C. Griffin, and C. Bottcher, *Phys. Rev. A* 32, 822 (1985).
23. K. Bhadra and R.J.W. Henry, *Phys. Rev. A* 26, 1848 (1982).
24. R.E.H. Clark, A. L. Merts, J. B. Mann, and L. A. Collins, *Phys. Rev. A* 27, 1812 (1983).

DISCLAIMER

This report was prepared as an account of work sponsored by an agency of the United States Government. Neither the United States Government nor any agency thereof, nor any of their employees, makes any warranty, express or implied, or assumes any legal liability or responsibility for the accuracy, completeness, or usefulness of any information, apparatus, product, or process disclosed, or represents that its use would not infringe privately owned rights. Reference herein to any specific commercial product, process, or service by trade name, trademark, manufacturer, or otherwise does not necessarily constitute or imply its endorsement, recommendation, or favoring by the United States Government or any agency thereof. The views and opinions of authors expressed herein do not necessarily state or reflect those of the United States Government or any agency thereof.